The starting mechanism study on rainfall-induced sloop loose source in strong earthquake area

Mingli Li (784189855@qq.com)
Chengdu University of Technology
Jianlong Cheng
Chengdu University of Technology

Research Article

Keywords: debris flow, rainfall, mechanical mechanism, loose slope source materials, startup

Posted Date: May 10th, 2022

DOI: https://doi.org/10.21203/rs.3.rs-1515905/v1

The starting mechanism study on rainfall-induced sloop loose source in strong earthquake area

Li Mingli; Cheng Jianlong*

Li Ming-li[1,2]: http://orcid.org/0000-0001-9458-6281; e-mail: 784189855@qq.com

Cheng Jian-long[1,2]*: http://orcid.org/0000-0001-9458-6281; e-mail: chengjl2018@foxmail.com

*Corresponding author

1 Chengdu University of technology, Chengdu 610059, China

2 State Key Laboratory of Geohazard Prevention and Geoenvironment Protection (Chengdu University of technology), Chengdu 610059, China

Abstract

Regarding risks from debris flows, previously unrecognized low-frequency loose slope source materials starting in formation areas constitute an especially significant threat. The 5.12 Wenchuan earthquake in 2008 led to a large number of loose deposits on the slope on both sides of the gully in the formation area. Under the triggering action of heavy rainfall, the gully easily failed and started earlier than the overall start of the gully debris flow, which has practical significance for realizing the early warning of the gully debris flow starting. The special loose source conditions and postearthquake geological environment change the hydraulic mechanism of traditional debris flow start-up, which brings great difficulties to the monitoring and early warning of postearthquake debris flows. Therefore, based on hydraulics, on the premise of building a hydraulic model of groundwater level change of loose slope accumulation body, the characteristics and rules of groundwater level change are analyzed with the aid of hydraulic seepage theories, and the action characteristics of hydrodynamic pressure and hydrostatic pressure on the accumulation body are quantitatively studied. Based on field exploration data and average slope gradient, we divided the accumulation body in a reasonable manner; completed the sliding force, anti-sliding force and residual-sliding force mechanical expression and establishment; and performed a slope stability analysis. The research results show that the slope-starting mode is divided into the thrust-type landslide and the retrogressive landslide mode of the subsection disintegration. The hydraulic deposit mechanism analytical results can also reverse the critical rainfall condition of slope failure. Finally, taking the Yindongzi gully in Dujiangyan as an example, the hydraulic mechanism of typical slope deposits in the formation area was analyzed and combined with the historical debris flow events in the study area to verify the physical simulation test, which was consistent with the field investigation results after the disaster.

Keywords: debris flow; rainfall; mechanical mechanism; loose slope source materials; startup

The Ms 8.0 The Wenchuan earthquake (Sichuan, China) occurred on May 12, 2008, resulting in 28×10^8 m^3 loose deposits. These gully sources and bank slope collapse accumulation bodies caused incessant debris flow disasters in the southwestern mountainous areas of China under the excitation of postearthquake heavy rainfall (Tang et al. 2012). On August 13, 2010, the torrential rain in the Longchi area of Dujiangyan led to the simultaneous outbreak of 48 debris flow gullies. On August 20, 2019, the Dujiangyan and Wenchuan areas were affected by subsequent rainstorms, resulting in group-occurring mountain torrents and debris flows (Jin et al.

2019). The sustained and combined effects of postearthquake secondary disasters are obvious. From 5 to 15 years after the earthquake, debris flow activities evolved into low-frequency, medium- and large-scale groups of sticky and transitional debris flows accompanied by mountain floods. Regarding risks from debris flows, previously unrecognized debris flow formation area loose sources on both sides of the gully bank in the upper basin constitute an especially significant threat (Zhao et al. 2020). On the one hand, because the forming region is located in a high valley, there is an abundant quantity of loose sources and a large longitudinal slope ratio; therefore, slope surface sources become the supply sources after slope failure. At the same time, the slope sources transport materials that further induce gully debris flows with high velocity, and slope source failure is highly invisible before outbreak and large chain destructiveness (Fan et al. 2008; Ouyang et al. 2019; Allaire et al. 2009; Gabet et al. 2006; Lourenço et al. 2015). On the other hand, heavy rainfall often occurs in southwestern mountainous areas during the flood season, and it takes time for the rain collection area above the formation area to form flow confluences and enter the debris flow gullies. Therefore, the failure of slope sources in formation areas is 10 to 15 minutes earlier than the start of the gully debris flows (Wang et al. 2016b; Ouyang et al. 2017; Lin et al. 2018). This short ten minutes is enough for common people to evacuate from the hazard range (Zhang et al. 2012; Zhang et al. 2013; Marcel et al. 2019). Therefore, it is of great realistic significance to understand the hydrodynamic conditions and mechanical mechanisms of gully bank slope sources to realize early warning and prediction of gully debris flow initiation.

Soil (void ratio, particle-size distribution, permeability coefficient, fine particle content, etc.), hydraulic (rainfall intensity, rainfall pattern), topographic and geomorphic conditions all affect the initiation of slope source materials (Shieh et al. 2009; Johnson et al. 1990; Marchi et al. 2002; Cannon et al. 2010). Under the sustained action of rainfall, the pore-water pressure increases, the soil shear strength correspondingly decreases, and the residual downward slippery force of the soil above the slope increases and accumulates continuously. When the down-sliding force is more than the anti-sliding force, the whole slope becomes unstable. When the slope body encounters heavy rainfall, the tip of the tensile crack in the slip band expands and deforms, and the pore-water pressure at the foot of the slope increases sharply, resulting in excess pore-water pressure formation, and the shallow landslide turns into a debris flow (Wen et al. 2005).

The sink flow produced by rainfall has the effects of bottom tearing and scouring, coercion, scraping and transporting of loose materials on the ditch bed replenishing the debris flow. Moreover, lateral erosion, devolution and dam breaks are also involved in the dynamic process of hydraulic debris flows (Zhuang et al. 2013; Gao et al. 2011). Cui (1992) carried out 48 groups of flow-scouring experiments in 1992, and the results showed that soil saturation, gully bed gradient and fine particle content jointly controlled the critical conditions for the initiation of hydraulic gully debris flow. Previous studies have been performed on soil-mechanical and hydraulic debris flows, and preliminary research on the mechanism of rock–soil masses with loose structural characteristics transforms into debris flows. However, these studies are not involved in the initiation problem of slope debris flows under special postearthquake conditions (Wu et al. 2012), and the relevant results could not meet the requirements of disaster prevention techniques for postearthquake reconstruction. The mechanical properties and particle composition of the loose postearthquake deposits have changed greatly compared with those before the earthquake. The postearthquake loose deposits on the gully bank slope have a wide range of sizes, from clay (particle size < 0.001 mm) to boulder (particle size > 100 mm), and are collectively called wide-grading loose soils (WGLS) (Guo et al. 2015). Wide-grading loose soils (WGLS) are a special slope deposit that often serve as a source for debris

flows in the western mountainous area of China and are mainly composed of gravel, soil, sand and block stone. WGLSs have a disorganized attitude, poor separation, loose structure, large void ratio and high permeability coefficient, and the corresponding hydraulic properties are very different from those of current water accumulation in regard to microstructure (Guo et al. 2020; Cui et al. 2017), which makes the traditional studies on debris flows starting difficult to interpret in regard to the problem of postearthquake debris flow initiation (Cui et al. 2019). Under the triggering action of heavy rainfall, the instability and movement of skeleton particles are mainly affected by seepage and flow scouring, and the movement of accumulated soil particles occurs as sliding with a small amplitude and then they become stable, transitional type sliding or rapid slip phenomena (Yang et al. 2014). The hydraulic mechanism of postearthquake loose deposit initiation is complex. The establishment of the hydraulic model of instability and the identification of the starting critical condition (rainfall threshold) can provide a theoretical basis for the early warning and prediction of postearthquake debris flows (Yang et al. 2019).

1. Hydraulic mechanism analysis of postearthquake loose slope source materials

The continuous priming action of steady-state heavy rainfall reduced the stability of the postearthquake slope in the formation area and eventually led to slope failure and further transformed into slope debris flows with a solid–liquid–vapor triphase. The initiation of slope failure is the result of water and soil coupling; therefore, it is necessary to combine the theories of soil mechanics, hydraulics and permeation fluid mechanics to reveal the mechanical mechanism of postearthquake slope material failure, which then further transforms into a debris flow.

1.1 Underground water level of slope materials formed by heavy rainfall

We set the steady-state rainfall intensity as I and the surface area of the slope or water-collecting area as S; then, the rainfall flow that infiltrates the whole slope is:

$$Q = IS \qquad (1\text{-}1)$$

The slope deposits in the southwestern mountainous area are mainly composed of gravelly soil, with a loose structure and a high permeability coefficient. When rainstorms occur in the flood season, heavy rainfall continuously infiltrates the slope, and the soil around the bedrock surface is saturated and generates a certain height H of free hydraulic head; that is, a diving level at a certain height. The accumulation body becomes unstable under hydraulic action and may eventually transform into a debris flow.

According to the Darcy law that can be applied in groundwater laminar flow, the seepage flow amount that rainfall infiltrates into the slope is directly proportional to the water level difference of the updown stream (elevation difference from the geoidal surface) and the wetted cross section and inversely proportional to the length of the seepage path:

$$Q = KA(H_2 - H_1)/L = KA\sin\theta \qquad (1\text{-}2)$$

where Q is the seepage quantity, $(H_2 - H_1)$ is water level difference of the updown stream, A is the cross-section area, which is perpendicular to the water flow direction, namely, the wetted area, L is the length of the seepage path, K is the permeability coefficient, and θ is the slope inclination angle. Figure 1 shows the hydrological model of loose slope deposits. We can infer that:

$$A = WH\cos\theta \qquad (1\text{-}3)$$

where W is the slope width and H is the depth of the diving level (Fig. 1). We bring Eq. (1-3) into Eq. (1-2) and we can obtain that:

$$Q = KWH\cos\theta \cdot \sin\theta \qquad (1\text{-}4)$$

By integrating Eq. (1-1) and Eq. (1-4), we can obtain:

$$H = \frac{IS}{KW\sin\theta\cos\theta} \qquad (1\text{-}5)$$

Theoretically, with continuous rainfall, the height of the groundwater level can be continuously raised until the slope is completely saturated (i.e., $H = Z$, where Z is the height of the slope), and eventually, surface runoff or excess infiltration surface flow is formed on the slope surface.

According to the hydraulics expression of runoff flux in saturated soil(Bishop et al. 1961; Lei et al. 2017), we can infer that:

$$Q_Z = TW\sin\theta \qquad (1\text{-}6)$$

where T is the transmissibility coefficient.

Then, by integrating Eq. (1-4) and Eq. (1-6), we can obtain:

$$K = \frac{T}{Z\cos\theta} \qquad (1\text{-}7)$$

We bring Eq. (1-7) into Eq. (1-5) and the formula can be simplified to obtain the groundwater level height generated in the slope after rainfall infiltration:

$$H = \frac{ISZ}{TW\sin\theta} \qquad (1\text{-}8)$$

According to Formula (1-8), the multivariate function relationship between groundwater depth and geometric parameters such as rainfall intensity, slope inclination angle and slope area is established. Groundwater is deeply affected by the above factors: the depth of the groundwater level (i.e., the height of the diving level) is positively proportional to rainfall intensity and slope height and inversely proportional to the transmissibility coefficient, slope width and slope inclination angle, and the depth of the groundwater level is mainly controlled by rainfall intensity.

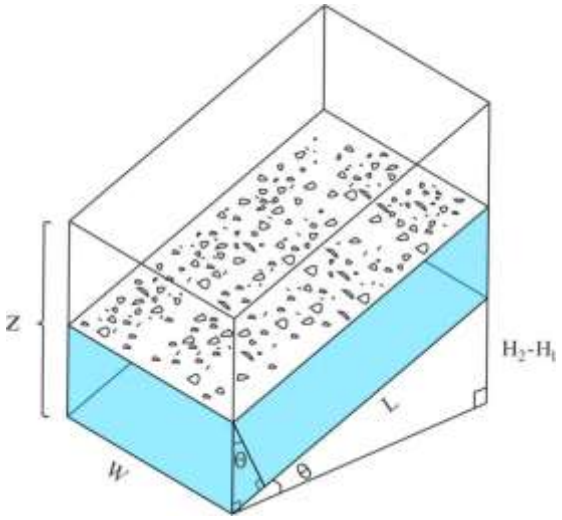

Fig. 1. The hydraulics model of slope deposits (CAD).

1.2 Analysis of the hydraulic mechanism of loose slope deposits

1.2.1 Hydrostatic pressure action

(1) Hydrostatic pressure

According to hydraulics, the height of the free water head at the upper entrance of the strip accumulation body is set as h_2, the free water head at the inferior outlet is set as h_1, and a coordinate system with the X direction along the gully bed and the Y direction perpendicular to the gully bed is established. Fig. 2 is a schematic diagram of the hydraulic function of the loose slope accumulation body.

According to the hydrostatic pressure at a point in the accumulation body(Montgomery et al. 1994; Wilkinson et al. 2002) $P = \gamma_w \cdot h$ (where γ_w is the unit weight of water in the accumulation body and h is the depth of underground water as well as the free water depth of this point), the osmotic hydrostatic pressure at a point along the X direction can be obtained as follows:

$$P_X = P_{h1} + \frac{x}{L}(P_{h2} - P_{h1}) \quad , x \in [0, L] \qquad (1\text{-}9)$$

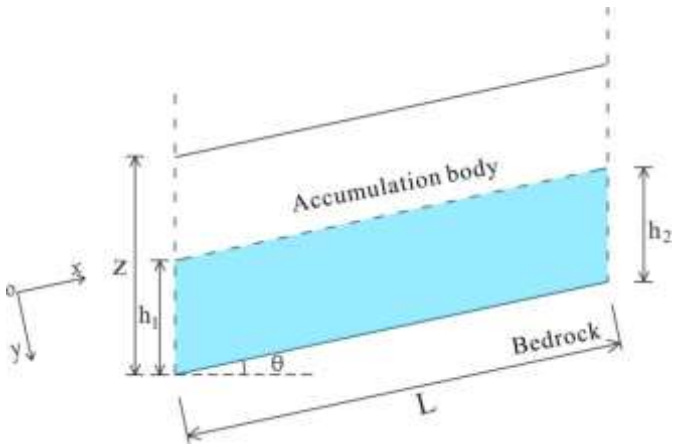

Fig. 2 The hydraulic function analysis of loose slope deposits at groundwater level.

By integrating P_{m} along the X-axis, the hydrostatic pressure of the strip accumulation body can be obtained:

$$P_{\mathrm{m}}=\int_0^L\left[P_{h_1}+\frac{X}{L}(P_{h_2}-P_{h_1})\right]dx=\frac{P_{h_1}+P_{h_2}}{2}L=\frac{\gamma_{\mathrm{w}}(h_1+h_2)}{2}L \quad \mathrm{x}\in[0,L] \qquad (1\text{-}10)$$

By setting $H_{\mathrm{m}}=\frac{h_1+h_2}{2}$, H_{m} is the average water depth of the strip accumulation body, and the hydrostatic pressure of the strip is:

$$P_{\mathrm{m}}=\gamma_w H_m L \qquad (1\text{-}11)$$

The hydrostatic pressure is an omnidirectional force and acts evenly on all parts of the slope surface. The average vertical compressive stress of phreatic flow on the bedrock surface of the accumulation body is:

$$\sigma_{\mathrm{wm}}=\gamma_w H_m \qquad (1\text{-}12)$$

1.2.2 Dynamic water pressure action

Postearthquake slope deposits with loose structures, large pores and grain compositions are given priority with gravel soil. When the rainfall intensity is large enough and the duration is long enough in the flood season, the groundwater level at a certain height is produced in the internal deposits. In the meantime, laminar flow occurs at the bottom of the deposit, which generates seepage dynamic water pressure. The effect of hydrodynamic pressure on the soil skeleton is presented in the form of a "drag".

According to the continuous media principle, the seepage dynamic water pressure at any point in the seepage zone is :

$$\vec{\boldsymbol{G}}_{\boldsymbol{d}}=\gamma_{\mathrm{w}}\vec{\boldsymbol{I}} \qquad (1\text{-}13)$$

where $\vec{\boldsymbol{G}}_{\boldsymbol{d}}$ and $\vec{\boldsymbol{I}}$ are the dynamic water pressure vector and hydraulic gradient vector, respectively.

Then, the seepage dynamic water pressure of laminar flow in the bedrock bottom to the slope accumulation body of unit width is:

$$G_{\mathrm{d}m}=\int_0^{H_m}\int_0^L\lambda\gamma_w I dxdy=\lambda L H_m\gamma_w I_m \qquad (1\text{-}14)$$

where λ is the void ratio of the loose deposits and $\mathrm{I_m}$ is the underground water hydraulic slope of the unit width loose slope deposits:

$$I_m=\frac{h_2+L\sin\theta-h_1}{L} \qquad (1\text{-}15)$$

The drag force of underground water on the slope accumulation body under seepage action is:

$$d_m = \frac{G_{dm}}{L} = \quad {}_wI_mH_m = \frac{{}_wH_m(h_2 + L\sin \quad h_1)}{L} \qquad (1\text{-}16)$$

When slope underground water flows through a loose accumulation body, the main internal and external causes of water head loss are the viscous action of rainwater and the friction resistance of the soil granular medium to slow waterflow, respectively. At this time, if the physical and permeability properties of the slope accumulation body are determined, the head loss η per unit flow distance of bottom laminar flow at low speed is determined or can be obtained by a response model test. Equation (1-14) can be simplified as:

$$G_{dm} = \lambda L H_m \gamma_w \eta \qquad (1\text{-}17)$$

Of course, for the whole loose slope accumulation, if the underground water head disappears before it flows out of the accumulation body, the drag effect of seepage water pressure of the hydraulic action mentioned above cannot be reflected. Assuming that the free water head at the top of the loose accumulation body is h_{m1} and the whole accumulation body is divided into m strips, the conditions for the bottom laminar flow on the bedrock surface (interface between bedrock and overburden) are as follows:

$$h_{m1} + \sum_{m=1}^{m=n} L_m \sin\theta_m - \sum_{m=1}^{m=n} \eta L_m \geq 0 \qquad (1\text{-}18)$$

1.3 Stress and stability analysis of slope accumulation bodies in formation areas under heavy rainfall conditions

By considering that the slope gradient of the postearthquake loose slope accumulation body is not uniform, the loose slope accumulation body can be further finely divided according to the slope change of the bedrock surface during the stress analysis to form multisegment unit strips, as shown in Fig. 3. Without considering shear and dislocation between each unit strip, the external forces that control the stability of the m section of the strip are gravity, the residual-sliding force between the strips, hydrostatic pressure, dynamic water pressure, supporting force of the bedrock surface and basal anti-sliding force. If the sliding force is greater than the anti-sliding force, the force system is balanced, and the accumulation body is stable.

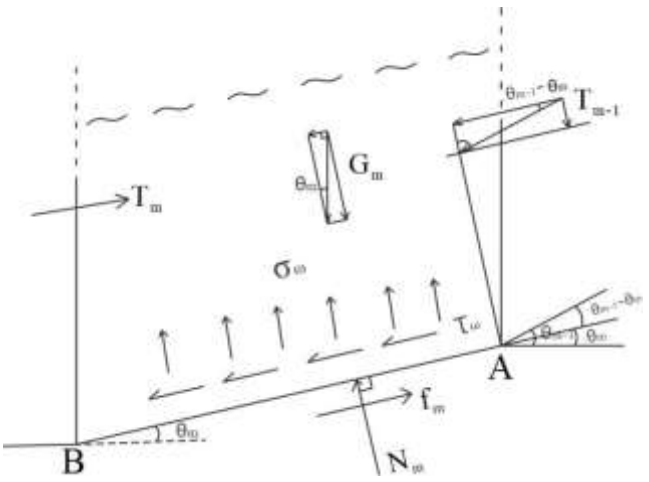

187 **Fig. 3. The force analytical schematic diagram of the unit loose accumulation body strip.**

188

189 According to the force analysis of strip M, the sliding force of the strip sliding along bedrock surface AB is:

$$S_m = G_m \sin\theta_m + T_{m-1}\cos(\theta_{m-1} - \theta_m) + G_{\mathrm{dm}} \qquad (1\text{-}19)$$

190 where S_{m} is the sliding force of the strip, G_{m} is the gravity of the strip m, and T_{m-1} is the
191 residual-sliding force of the previous strip $m-1$. In particular, when $m=1$, the initial strip has no
192 residual-sliding force T_{m-1} from the previous strip; similarly, when $m=n$, the unit strip is at the bottom of
193 the accumulation body, and there is no reaction force T_{m} of the next strip $m+1$, namely:

$$\begin{cases} T_0 = 0 \\ T_{\mathrm{m}} = 0 \end{cases} \qquad (1\text{-}20)$$

194 The sliding force acting on the strip m is:

$$F_m = T_m + f_m \qquad (1\text{-}21)$$

195 where T_m is the reaction force of the next strip and f_m is the basal anti-sliding force of the strip m. In
196 1773, Coulomb proposed the Moore–Coulomb yield criterion:

$$\tau_{\mathrm{w}} = c + \sigma_w \tan\varphi \qquad (1\text{-}22)$$

197 where c is the cohesion of the loose accumulation soil, φ is the internal friction angle of the loose
198 accumulation soil, and τ_{w} and σ_w are the shear stress and normal stress on the slip surface, respectively. By
199 combining the hydrostatic pressure formula (1-9), we can obtain the following:

$$\tau_{\mathrm{w}} = \frac{f_{\mathrm{m}}}{L} = c + \frac{\left[G_m\cos\theta_m + T_{m-1}\sin(\theta_{m-1}-\theta_m) - \gamma_w H_m L\right]}{L}\tan\varphi \qquad (1\text{-}23)$$

200 After simplification, we can obtain:

$$f_{\mathrm{m}} = \mathrm{c}L + \left[G_m\cos\theta_m + T_{m-1}\sin(\theta_{m-1}-\theta_m) - \gamma_w H_m L\right]\tan\varphi \qquad (1\text{-}24)$$

201 According to the force analysis of the accumulation body, the condition for the stability of the loose
202 accumulation body unit strip m is $F_{\mathrm{m}} \geq S_m$; in theory, strip 1 to strip m are all stable. Especially when the
203 strip n of the loose accumulation body still meets the condition $F_n \geq D_n$, the whole accumulation body is in the
204 overall stable state. In contrast, when the unit strip accumulation body m is stable while the unit strip
205 accumulation body n is unstable, the loose accumulation body on the slope surface will partially start. In the
206 meantime, the unit strip accumulation body n must also meet the condition: $f_n < S_n$.

2 Case study of monitoring data in the study area

2.1 Profile of the study area

To verify the theory of hydraulic mechanism analysis in this paper, the Yindongzi gully in Dujiangyan city is taken as an example. The Yindongzi debris flow gully is located in Longchi town, Dujiangyan city, which is a serious disaster area of the Wenchuan earthquake. The geographic location coordinates of the gully mouth are 103°40 '19" E and 31°9' 46" N, and the elevation is 1070~2 2050 m. It belongs to the tectonic erosion landform of Zhongshan Canyon. The mountain trend is mostly toward the northeast and southwest, and the crest is narrow. The general terrain slope gradient is between 30° and 55°, and the valley cutting is deep, steep above and slow at the bottom, and is mostly a "V"-type valley.

The exposed strata in the gully consist of bedrock and Quaternary loose deposits, among which bedrock contains granite, andesite, diorite, tuff and some metamorphic rocks of the Sinian lower series volcanic rock group (Z_a). The Quaternary strata consist of Holocene residual-slope accumulation (Q_4^{el+pl}), diluvial-slope deposits (Q_4^{pl+dl}) and colluvial-slope deposits (Q_4^{col+dl}), which are dominated by loose wide-graded gravel soils with a thickness of approximately 1~20 m. The thickness of deposits varies greatly, generally having thin ridges and thick gullies, and there are a total of 5 deposit bodies on both sides of the gullies, which can provide abundant loose materials for debris flow initiation. The area of Yindongzi gully is approximately 2.2 km^2, the overall length of the main gully is 2.5 km, the average longitudinal slope declination of the main gully is 310‰, the total material source volume of the gully is 83.55×10^4 m^3, and the dynamic reserve volume on the slope that can participate in debris flow activity is 23.02×10^4 m^3 (Fig. 4).

The clear water area of the Yindongzi debris flow gully is a funnel-shaped terrain surrounded by mountains on three sides and an exit on one side. The formation area elevation is 1560 m-1330 m, the gully is 813 m long, the rainwater collecting area is 0.35 km^2, the gully is deep, the terrain is steep, the valley slope is 45°-75°, and the average longitudinal slope decline is 283‰. This terrain condition enables the rapid and straight downward flow of debris flows; moreover, the formation area materials start earlier than the gully debris flow. Therefore, the four loose source deposits in the formation area are the key research objects of this study, which can realize the early warning of gully debris flows. The circulation area is the coseismic landslide of the Wenchuan earthquake. The accumulation area has a 7° slope and is located at the mouth of Yindongzi gully, with a total volume of 2.8×10^4 m^3 consisting of a loose accumulation body. On the right side of the accumulation fan at the gully mouth of the debris flow, the postdisaster reconstruction resettlement site of Lianhe Village of Hongkou Township was built. Fifty-six families and 228 residents are planned to be settled in the resettlement site, which is adjacent to the Baisha River watershed.

The study area has abundant rainfall but uneven spatial and temporal distributions. The annual mean rainfall in recent years was approximately 1100 mm, and the maximum rainfall in one day was 183.2 mm (2010.8.13). There are frequent rainstorms and concentrated rainfall in the flood season, which provides hydrodynamic conditions for the start of slope source materials. The potential danger of debris flows is medium, which poses a great threat to the lives and property safety of more than 200 people(Yang et al.2017).

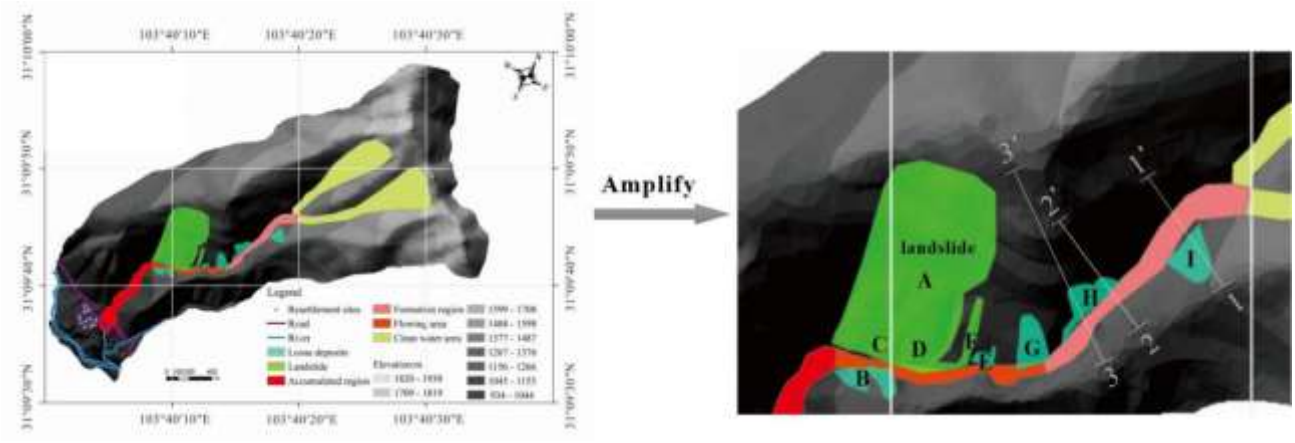

Fig. 4. Topographic map of the Yindongzi debris flow gully (1:500).

Fig. 5. The accumulation fan in the gully mouth and postdisaster reconstruction site.

2.2 Case study on the hydrodynamic mechanism of postearthquake slope source materials

Before starting the mechanism study of postearthquake slope source materials, a detailed field investigation and geological exploration work of the Dujiangyan Yindongzi debris flow gully were carried out, and precise mapping and exploratory trench excavation were performed on the whole basin. In addition, the geological and geomorphic elements of slope sources in the formation area were calculated and counted in detail on a topographic map at a scale of 1:1000 (Fig. 5) to explore the distribution, reserves, morphology and other characteristic elements of loose source deposits. To study the starting pattern and conditions of the postearthquake loose accumulation body under the rainfall excitation action, the stress calculation and analysis of the slope above the formation area where Section Plane 3-3' is located are shown in Fig. 5 and Fig. 6. According to the field geological survey, the slope body is 23.07-115.96 m wide and 326.7 m long, with an area of approximately 5000 m^2 and a slope of 8.16°-45.34°. The slope is mostly a loose landslide accumulation body, which is thin on the top and thick on the bottom and is unstable at present. Based on the geological sectional drawing of the accumulation body, it can be divided into AB, BC, CD, DE and EF 5 sections from top to bottom according to the average width, slope gradient and accumulation thickness, as shown in Fig. 7 and Fig. 8, and relevant calculation parameters are shown in Table 1 and Table 2.

Fig. 6. Loose deposits at the foot of the slope in the study area.

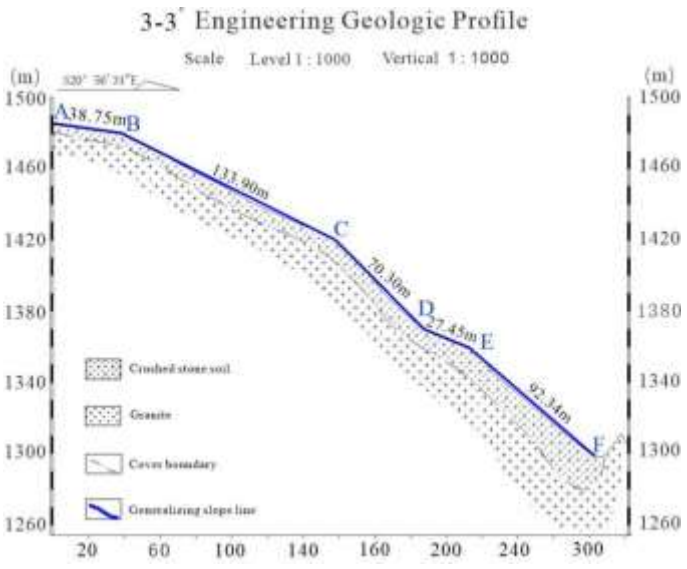

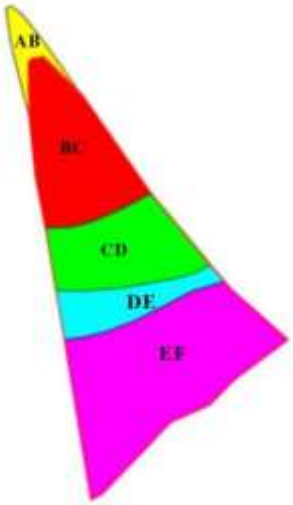

Fig. 7 Cross-section diagram of loose deposits at Section Plane 3-3. Fig. 8 Strip division of loose slope deposits.

Table 1 Geometric parameters of the loose slope deposits of the H landslide.

m	Segmentation	L_m/m	W_m/m	Z_m/m	θ_m/°
1	AB	38.75	23.07	5.50	8.16
2	BC	133.90	42.33	60.00	26.62
3	CD	70.30	66.15	50.00	45.34
4	DE	27.45	87.83	10.50	22.49
5	EF	92.34	115.96	60.50	40.93

Table 2 Mechanical parameters of postearthquake loose slope deposits.

Internal friction angle	Pore ratio of accumulation body	Head loss of unit length	Cohesion	Transmissibility coefficient	Unit weight of accumulation body	Unit weight of groundwater
φ/（°）	λ	η	c/kPa	T/(m^2/h)	γ^s/(kN/m^3)	γ^w/(kN/m^3)
34.1	0.42	0.24	10.15	301	18.9	9.8

2.2.1 Variation law of groundwater level height and hydraulic power of slope accumulation body under the rainfall effect

According to the geometric and mechanical parameters of the loose slope accumulation body in the study area (Table 1 and Table 2), combined with Equations (1-8), the groundwater level depth of the accumulation body in each section under different steady rainfall intensities can be calculated. It is necessary to further explain that Slope 3-3' in the study area is divided into five sections according to the average slope gradient. The first section accumulation body is located at the top of the slope; therefore, the rainfall collecting area is the section rainfall receiving area as well as the slope surface area. The second accumulation body is the sum of the rainfall collecting area of the previous section accumulation body and the area of the current accumulation body on the slope. Classification grades based on rainfall intensity include light rain (<10 mm/d), moderate rain (10-25 mm/d), heavy rain (25-50 mm/d), rainstorm (50-100 mm/d), severe rainstorm (100-250 mm/d) and severe torrential rain (>250 mm/d). Fig. 9 shows the groundwater level depth of accumulation bodies in each section under different steady-state rainfall intensities.

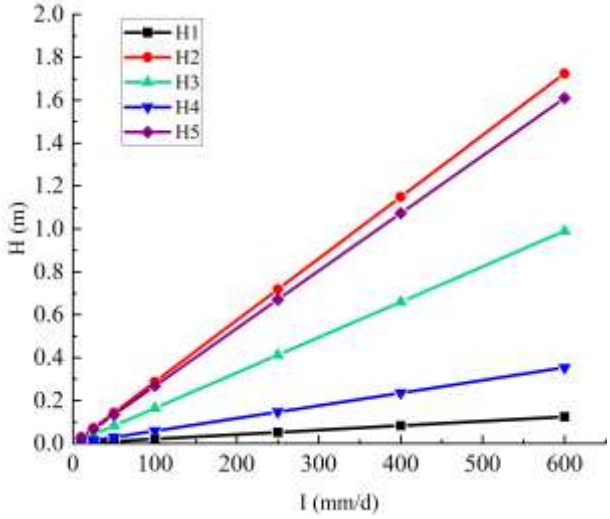

Fig. 9. The groundwater level depth of the slope accumulation body at different positions under different rain intensity conditions.

Theoretically, with the increase in rainfall intensity, the height of groundwater level H in the accumulation

body will increase until it exceeds the height of the accumulation body to form surface runoff. However, due to the large thickness of the slope accumulation body in the study area, there will be no groundwater exposure under the condition that the severe torrential rainfall intensity is 600 mm/d. When the slope gradient is smaller, the slope surface is narrower and the deposit is thicker, the groundwater level will be higher, and the influence of the catchment area will be largest, resulting in Section 2 producing the highest groundwater level due to the dip length and catchment area of deposit BC being the largest. Meanwhile, deposit section AB with minimum catchment area AB produced the lowest groundwater level. Second, the groundwater level height is also highly sensitive to the slope gradient, which results in the accumulation body in the third Section CD and fifth Section EF having the largest slope gradient, producing a higher groundwater level height.

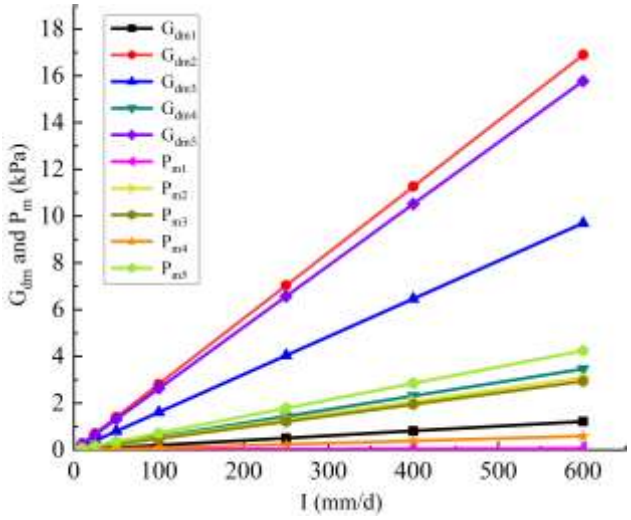

Fig. 10. Hydraulic variation rule of the slope accumulation body under different rainfall conditions.

If the groundwater level height of deposits under different rainfall conditions varies, then hydraulic function also changes. By Formulas (1-16), we can determine that the groundwater of the accumulation body will experience laminar flow and seepage effects of dynamic hydraulic pressure in the form of a drag effect, and the entire deposit dynamic hydraulic pressure is far less than the hydrostatic pressure (Fig. 10). This indicates that the instability of postearthquake loose slope deposits is the main result of hydrostatic pressure change and groundwater level raising. As the rain intensity continues to increase, theoretically, hydrostatic pressure, dynamic hydraulic pressure and other hydraulic characteristics will remain constant only when groundwater flows out.

2.2.2 The starting force analysis of postearthquake loose slope source materials

Combined with the stress stability analysis of the accumulation body in 1.3, the critical conditions, start-up pattern and stability of the loose accumulation body in Dujiangyan Yindongzi gully are analyzed and calculated. If the remaining sliding force is negative, it indicates that the accumulation body in this section is self-stable and that there is anti-sliding reserve. In this case, the accumulation body is stable, and the force on the next section of the accumulation body is written as 0. The calculation results are shown in Table 3 and Table 4. Under the rainfall condition of severe torrential rain, the residual-sliding force of the Section 1 accumulation body is still negative, indicating that this accumulation body can be self-stable, will not start, and cannot be used as a debris flow source to start and supply the dynamic reserves of the gully source. From the longitudinal perspective of Table 3 and Table 4, rainfall intensity and slope gradient have the greatest influence on slope stability. For the same section of

accumulation body. When the rainfall intensity increases, the sliding force increases, and the anti-sliding force continues to increase due to the growth of the dead weight, but the growth rate of the anti-sliding force is less than that of the sliding force, leading to a gradual increase in the residual-sliding force. Table 3 and Table 4 show that slope is mostly sensitive to slope stability. According to the slope gradient of the deposits in Table 1, the accumulation body slope gradient of Section 3 and Section 5 are both greater than 40°, and it is difficult to achieve self-stability even under the very small rainfall intensity condition. The slope of the Section 4 accumulation body is again gentle (22.49°), resulting in the remaining sliding force between Section 3 and Section 4; furthermore, these results demonstrate that Section 4 resisted part of the pushing force from the previous section of the accumulation body.

Table 3 Stress values of accumulation bodies under different rainfall conditions.

I	S_1	S_2	S_3	S_4	S_5	f_1	f_2	f_3	f_4	f_5
10	13.19	2880.19	4878.154	3854.81	11340.85	16.86	1030.15	660.04	356.43	1855.22
25	13.19	2880.52	4878.61	3855.19	11342.01	16.86	1030.25	660.1	356.46	1855.41
50	13.19	2881.07	4879.37	3855.82	11343.93	16.87	1030.43	660.18	356.52	1855.71
100	13.2	2882.16	4880.89	3857.09	11347.77	16.87	1030.77	660.36	356.65	1856.32
250	13.21	2885.44	4885.44	3860.88	11359.3	16.88	1031.8	660.87	357.01	1858.13
400	13.22	2888.72	4889.98	3864.67	11370.83	16.89	1032.83	661.39	357.38	1859.95
600	13.24	2893.08	4896.05	3869.73	11386.2	16.91	1034.21	662.08	357.87	1862.37

Table 4 Residual-sliding force under different rainfall conditions.

I (mm/d)	T_1	T_2	T_3	T_4	T_5
10	-3.67	1850.04	6068.15	9566.54	19052.17
25	-3.67	1850.27	6068.78	9567.51	19054.11
50	-3.67	1850.64	6069.83	9569.13	19057.35
100	-3.67	1851.39	6071.92	9572.36	19063.82
250	-3.67	1853.64	6078.20	9582.07	19083.24

400	-3.67	1855.88	6084.47	9591.77	19102.65
600	-3.67	1858.87	6092.84	9604.70	19128.53

Note: In Table 3 and Table 4, the unit of rainfall intensity I is mm/d, S_m is the sliding force, f_m is the basement anti-sliding force, T_m is the residual-sliding force, and the units of the above three factors are 10^6 N. When T_m is negative, it indicates that the accumulation body can be self-stable and has no force effect on the next section of the accumulation body.

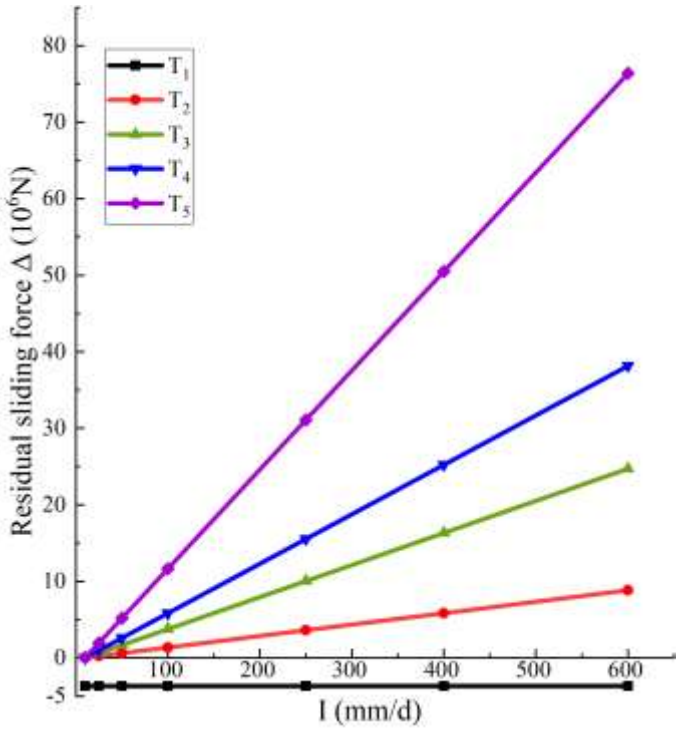

Fig. 12. Change regulation of the hydraulic action of the accumulation body at different groundwater levels.

Figure 12 shows the variation regulation of the residual-sliding force under different rainfall conditions, and Δ is the difference value between the residual-sliding force in this section and the minimum values under different rainfall conditions (except Section 1). Section 1 of the deposit will realize a self-stable state under any rainfall condition under different rainfall intensities. Deposits 2 to 5 are particularly unstable, and they will lose anti-sliding reserves under light rainfall intensity conditions. As a result, the consecutive and integral instability of Section 2 to Section 5 of accumulation bodies and this type of starting pattern represents typical thrust-type instability. Theoretically, if Section m of the accumulation body is stable and Section m+1 of the deposit starts, then the loose accumulation body starts in sections by disintegration and evolves into a debris flow, which is a typical overall thrust-type failure.

3. Comparison and verification of historical debris flow events in the study area and hydraulic mechanism analytical results

According to the above stress analytical results, the first section of the accumulation body is stable, while Sections 2 to 5 are in an extremely unstable state. The Yindongzi debris flow gully in Dujiangyan started 15 times

after the earthquake, including the 7.17 debris flow in 2009, 8.13 debris flow in 2010, and 7.9 debris flow in 2013 (Table 5). Although the lowest rainfall in 24 hours was 39 mm/d (2011.9.6), the gully debris flow could be started at a full-scale. A topographic map (Fig. 4) was explored in July 2016, and monitoring instruments, such as rain gauges, pore pressure and moisture content sensors, surface tiltmeters and video monitors, were installed in the study area. From August 18 to 19, 2017, and August 24 to 25, 2017, the city of Dujiangyan had two obvious regional rainstorm weather processes (the former referred to as the "8.18" rainstorm, the latter referred to as the "8.24" rainstorm). The rainfall of the 8.18 rainstorm was up to 156 mm/d in 24 hours, and the accumulated rainfall of the 8.24 rainstorm was up to 178 mm. According to the field investigation after the disaster, except for a small part of the upper accumulation body of slope accumulation body H in the formation area that was "self-stable" (Section 1), the rest of the slope accumulation body (Section 2 to Section 5) were all started. Under such rainfall conditions, the starting and instability failure state of accumulation body H was completely consistent with the calculation results in Section 2.2.2. In addition, because the rainfall over 24 hours was heavy, water gushed out at the bottom of the slope (Fig. 14) and converged into a high-speed water flow with a width of approximately 1 m in the gully (Fig. 15). Field investigation results after the disaster showed that rainfall led to the formation of a groundwater level with a certain height in the accumulation body. According to the height of the mud trace on both sides of the gully, the overflow height was approximately 6 m, and the maximum flood flow velocity was approximately 100 m3/s. After the debris flow, the total amount of accumulation below the ditch mouth reached 6×104 m3, and the deposit amount in the gully above the ditch mouth reached 9×104 m3, which represents a large-scale debris flow. The debris flow did not destroy the houses of the settlement site, the road through the village was buried, the rainfall early warning signal was issued in time, and people safely evacuated without casualties. The debris flow event resulted in severe damage to the gravity dam, drainage canal and monitoring equipment.

Table 5 Historical events of the Yindongzi debris flow gully.

Date	Disaster characteristics and starting time	Rainfall in 24 h （mm）	Accumulated rainfall（mm）
2009.7.17	Group-occurring debris flow in Hongkou township.	97.40	219.00
2010.8.13	Group-occurring debris flow in Hongkou township.	183.20	275.10
2010.8.19	Group-occurring debris flow in Hongkou township.	98.00	150.00
2011.07.21	Rainstorm，debris flow occurred	65.10	95.10
2011.08.15	A small amount of debris flow appeared at 4:30 a.m.	42.00	61.70
2011.08.16	The debris flow occurred at 9:15 a.m. and 4:23 p.m., respectively.	49.00	110.70
2011.08.21	The debris flow occurred at 2:30 a.m.	144.80	150.10
2011.09.06	The debris flow occurred at 5:30 a.m.	39.00	66.60
2012.08.18	The debris flow occurred at night.	105.60	206.00

2012.08.19	The debris flow reached the Baisha River.	41.90	247.90
2013.07.08	A large amount of debris flow rushed out.	111.60	163.90
2013.07.09	A large amount of debris flow rushed out.	217.20	409.50
2013.07.26	The debris flow occurred at 5:30 a.m.	108.80	235.00
2013.07.29	A large amount of debris flow rushed out.	128.10	403.00

Figure. 13 Before and after accumulation body H morphological comparison of the 8.24 debris flow in the study area.

Figure. 14 Clear water gushing from the bottom of the H slope foot.

Figure. 15 High-speed flow at a large landslide downstream and in the circulation area.

4. Large physical model experimental verification

Li Mingli (2018) used more than 20 groups of artificial rainfall physical test methods to set rainfall intensity and slope gradient as control variables and studied four slope types (32°, 34°, 37° and 42°) under five rainfall intensity conditions (60 mm/h, 90 mm/h, 120 mm/h, 150 mm/h, and 180 mm/h), the instability mechanism and failure mode of loose source materials on slope surfaces. According to the critical condition of slope start-up,

382 regression analysis of test results was conducted by using mathematical statistical methods. The multiparameter
383 early warning model and rainfall threshold of 24 h cumulative rainfall were proposed as 180.2 mm/d. The
384 experiments showed that the slope gradient was positively correlated with the slope starting rainfall intensity.
385 Under a slope condition of 32° -37° medium degree, the slope source materials were fully activated, and above 37
386 degrees slope, an integral failure mode dominated the slope starting, while a certain height of groundwater level
387 was generated. When the 8.18 and 8.24 rainstorms occurred, each section failure state of accumulation body H and
388 the height of the groundwater level generated in the slope were consistent on the one hand with the calculation
389 results of the hydraulic mechanism (2.2.1) and on the other hand verified the field investigation results after the
390 disaster (2.2.3).

391

392 **5. Discussion**

393 This paper is based on hydrology, on the premise of constructing a hydraulic model of groundwater level
394 variation in a loose accumulation body, and with the aid of hydraulic theory, the change in hydraulic
395 characteristics and the variation in hydraulic power with increasing groundwater level were analyzed. Furthermore,
396 the mechanical expression of rainfall infiltration on the accumulation body was constructed, the stability of the
397 slope was analyzed, and the critical condition of source instability and the mechanical prediction model were
398 obtained.

399 The research object is the postearthquake loose slope source materials in the formation area, and the
400 application scope of the hydraulic model is postearthquake wide-grading loose soils (WGLS) with a large void
401 ratio and high permeability coefficient in the mountainous area of Southwest China. The physical and mechanical
402 properties of this kind of crushed soil are quite different from those before the earthquake, and the interior of the
403 slope body forms a groundwater level of a certain height under the excitation action of steady heavy rainfall.
404 Different from the shallow surface landslides of the rainfall type, the postearthquake slope source starting is the
405 result of the combined action of hydrostatic pressure and hydrodynamic pressure, and before the slope starts, the
406 hydraulic condition continuously deteriorates, which belongs to the hydraulic class starting form.

407 Studies of hydraulic-type gully debris flows have become more mature, and the failure time of slope source
408 materials on both sides of gully banks in watershed formations was earlier than the comprehensive start of gully
409 debris flows. The hydraulic analyses of postearthquake slope source materials not only prove the hydraulic
410 mechanism of slope source initiation but also invert the critical steady rainfall condition of its initiation, which has
411 practical and feasible significance for realizing the early warning of gully debris flow initiation. The results of the
412 theoretical analysis, historical debris flow events in the study area, physical model test results and real-time field
413 monitoring data of the postearthquake slope source materials in the formation area were compared and analyzed.
414 The results are basically consistent, and the results of hydraulic mechanism analysis are relatively reliable. The
415 study area of the Yindongzi debris flow gully has detailed geological exploration content and rich historical debris
416 flow data; at the same time, field monitoring work has lasted for ten years, the typical geological disaster site field
417 monitoring work is ongoing and will continue for a long time, and primary field monitoring data will constantly
418 improve and effectively modify slope source starting hydraulic models.

419

6. Conclusions

(1) The postearthquake slope source materials are mainly gravel soil, which has the characteristics of wide-grain grading and a large permeability coefficient. The instability of loose slope accumulation bodies is the result of the continuous increase in groundwater level and deterioration of hydraulic conditions under the triggering action of heavy rainfall.

(2) According to the theoretical derivation of hydraulics and soil mechanics, the height of the groundwater level generated in the accumulation body is a comprehensive function of parameters such as slope rainfall area S, steady-state rainfall intensity I, slope geometric parameters (W, H, Z) and transmissibility coefficient T. For the physical and geometric properties of the slope accumulation body, the larger S and I are, the higher the height of groundwater level H; conversely, the larger T, W and Z are, the lower the height of groundwater generated in slope body Z. Generally, the narrower the slope is, the deeper the accumulation body thickness, the larger the slope surface area, and the greater the loose accumulation body instability, which further translates into debris flows.

(3) In terms of the two hydraulic effects caused by the uplift of the groundwater level, on the one hand, the increase in hydrostatic pressure P in the slope reduces the anti-sliding force of the base of the accumulation body; on the other hand, the increase in hydrodynamic pressure Gd increases the sliding force that causes slope failure. However, the effect of hydrodynamic pressure on the loose accumulation body instability after rainfall is relatively small.

(4) According to the existence form of the remaining sliding force, the starting mode of the postearthquake loose slope accumulation body can be divided into two types: the sliding mode of the thrust-type landslide and the retrogressive landslide mode of the subsection disintegration. Taking the case of the Yingdongzi gully as an example, except for Section 1 of the accumulation body, the residual-sliding force of the accumulation body of Section 2 to Section 5 continuously accumulated downward, presenting a starting mode of overall thrust-type failure.

Acknowledgments The authors also gratefully acknowledge support from the State Key Laboratory of Geohazard Prevention and Geoenvironment Protection, the Independent Research Project (SKLGP2020Z004) and the National Natural Science Foundation of China (Grant Nos. 42107179 and 42077245).

Funding The research was supported by the National Key Research and Development Program of China (2018YFC1505402).

References

(1) Allaire SE, Roulier S, Cessna AJ. (2009) Quantifying preferential flow in soils: A review of different techniques. Journal of Hydrology, 378(1-2): 179-204.

(2) Bishop AWT, Alpan I, Blight GE. (1961) Factors controlling the strength of partly saturated cohesive soils. Rearch Conference on Shear Strength of Cohesive Soil. ASCE.

(3) Cannon SH, Bigio ER, Ming E. (2010) A process for fire‐related debris flow initiation, Cerro Grande fire, New Mexico. Hydrological Processes: 15.

(4) Cui P. (1992) Study on conditions and mechanisms of debris flow initiation by means of experiment. Chinese

Science Bulletin, 37(9): 759-759.

(5) Cui YF, Yao J, Guo CX. (2019) Investigation of the initiation of shallow failure in widely graded loose soil slopes considering interstitial flow and surface runoff. Landslides, 16(4): 815-828.

(6) Cui YF, Zhou XJ, Guo CX. (2017) Experimental study on the moving characteristics of fine grains in wide grading unconsolidated soil under heavy rainfall. Journal of mountain science, 14(3): 417-431.

(7) Fan XM, Juang CH, Wasowski J, et al. (2018) What we have learned from the 2008 Wenchuan Earthquake and its aftermath: A decade of research and challenges. Engineering Geology 241: 25-32.

(8) Gabet EJ, Mudd SM. (2006) The mobilization of debris flows from shallow landslides. Geomorphology, 74(1/4): 207-218.

(9) Gao B, Zhou J, Zhang J. (2011) Macro-meso analysis of water-soil interaction mechanism of debris flow starting process. Chinese journal of rock mechanics and engineering, 30(12): 2567-2573. (In Chinese)

(10) Guo CX, Cui YF. (2020) Pore structure characteristics of debris flow source material in the Wenchuan earthquake area. Engineering Geology, 267(1): 105499.

(11) Guo XJ, Cui P, Li Y, et al. (2016) Spatial features of debris flows and their rainfall thresholds in the Wenchuan earthquake-affected area. Landslides, 13(5): 1215-1299.

(12) Hürlimann M, Coviello V, Bel C, et al. (2019) Debris-flow monitoring and warning: review and examples. Earth-Science Reviews: 102981.

(13) Jin W, Zhang GT, Zou Q, et al. (2019) A New Understanding of the Activity Behavior of Post-earthquake Debris Flow——Taking the“8·20”Event in Wenchuan,Sichuan,China as an Example. Mountain research 37(5): 787-796. (In Chinese)

(14) Johnson KA, Sitar N. (1990) Hydrologic conditions leading to debris-flow initiation. Canadian Geotechnical Journal, 27(6): 789-801.

(15) Lei XQ, Yang ZJ, He SM, et al. (2017) Numerical investigation of rainfall-induced fines migration and its influences on slope stability. Acta Geotechnica, 12: 1431-1446.

(16) Li ML, Jiang YJ, Yang T, et al. (2018) Early warning model for slope debris flow initiation. Journal of mountain science, 15(006): 1342-1353.

(17) Lin HM, Wu JH, Sunarya E. (2018) Consolidated and Undrained Ring Shear Tests on the Sliding Surface of the Hsien-du-shan Landslide in Taiwan. Geofluids: 1-12

(18) Lourenço SDN, Wang GH, Kamai T. (2015) Processes in model slopes made of mixtures of wettable and water repellent sand: Implications for the initiation of debris flows in dry slopes. Engineering Geology, 196: 47-58.

(19) Marchi L, Arattano M, Deganutti AM. (2002) Ten years of debris-flow monitoring in the Moscardo Torrent (Italian Alps). Geomorpholog, 46(1): 1-17.

(20) Montgomery DR , Dietrich WE. (1994) A physically based model for the topographic control on shallow landsliding. Water Resources Research, 30(4): 1153-1171.

(21) Ouyang CJ, An HC, Zhou S, et al. (2019) Insights from the failure and dynamic characteristics of two sequential landslides at Baige village along the Jinsha River, China. Landslides 16: 1397-1414.

(22) Ouyang CJ, Zhou KQ, Xu Q, et al. (2017) Dynamic analysis and numerical modeling of the 2015 catastrophic landslide of the construction waste landfill at Guangming, Shenzhen, China. Landslide. Landslides, 14 (2): 705–718.

(23) Shieh CL, Chen YS, Tsai YJ, et al. (2009) Variability in rainfall threshold for debris flow after the Chi-Chi earthquake in Central Taiwan, China. International Journal of Sediment Research, 24: 177-188.

(24) Tang C, Van Asch, T.W.J, Chang M, et al. (2012) Catastrophic debris flows on 13 August 2010 in the Qingping area, southwestern China: The combined effects of a strong earthquake and subsequent rainstorms. Geomorphology 139–140(1): 559-576.

(25) Wang ZB, Li K, Wang R, et al. (2016) Impact of fine particle content on mode and scale of slope instability of debris flow. Advances in Science and Technology of Water Resources, 36(2):35-41. (In Chinese)

(26) Wen BP, Aydin A. (2005) Mechanism of a rainfall-induced slide-debris flow: constraints from microstructure of its slip zone. Engineering Geology, 78(1-2): 69-88.

(27) Wilkinson PL, Anderson MG, Lloyd DM, et al. (2002) Landslide hazard and bioengineering: Towards providing improved decision support through integrated numerical model development. Environmental Modeling and Software, 17(4): 333－344.

(28) Wu Y, He SM, Pei XJ, et al. (2012) Analysis of condition of startup of gully debris flow after earthquake-The hydraulic mechanism of instability of loose deposits in rainfall. Rock and soil mechanics, 33(010): 3043-3050. (In Chinese)

(29) Yang S, Ou GQ, Wang J, et al. (2014) Experimental analysis of scouring of debris flow initiation process under steady seepage condition. Rock and soil mechanics, 035(012): 3489-3495. (In Chinese)

(30) Yang ZJ, Cai H, Shao W, et al. (2019) Clarifying the hydrological mechanisms and thresholds for rainfall-induced landslide: in situ monitoring of big data to unsaturated slope stability analysis. Bulletin of engineering geology and the environment, 78(4): 2139-2150.

(31) Yang ZJ, Qiao JP, Uchimura T, et al. (2017) Unsaturated hydro-mechanical behaviour of rainfall-induced mass remobilization in post-earthquake landslides. Engineering geology, 222: 102–110.

(32) Zhang H, Liu X, Cai E, et al. (2013) Integration of dynamic rainfall data with environmental factors to forecast debris flow using an improved GMDH model. Computers & Geosciences, 56: 23-31.

(33) Zhang JS, Cui P. (2012) Research on and implementation of debris-flow forecast and warning. Journal of Hydraulic Engineering, 43: 174-180. (In Chinese)

(34) Zhao Y, Meng XM, Qi TJ, et al. (2020) Ai-based identification of low-frequency debris flow catchments in the bailong river basin, China. Geomorphology 359: 107125-.

(35) Zhuang JQ, Cui P, Peng JB, et al. (2013) Initiation process of debris flows on different slopes due to surface;

524 flow and trigger-specific strategies for mitigating post-earthquake in;old Beichuan County, China. Environmental
525 Earth Sciences, 68(5): 1391-1403.
526
527
528